A Current Sensorless Delay–Based Control Scheme for MPPT–Boost Converters in Photovoltaic Systems

José-Enrique Hernández-Díez, César Fernando Méndez Barrios, Silviu-Iulian Niculescu, Ernesto Bárcenas-Bárcenas

HAL Id: hal-02950794

https://hal.science/hal-02950794v1

Submitted on 9 Mar 2021

IEEE *Access*

A Current Sensorless Delay–Based Control Scheme for MPPT–Boost Converters in Photovoltaic Systems

JOSÉ-ENRIQUE HERNÁNDEZ-DÍEZ[1,2], CÉSAR-FERNANDO MÉNDEZ-BARRIOS[2], SILVIU-IULIAN NICULESCU[1] AND ERNESTO BÁRCENAS-BÁRCENAS.[3]

[1]University Paris-Saclay, CNRS, CentraleSupélec, Laboratoire des Signaux et Systèmes (L2S, UMR CNRS 8506), Inria team "DISCO",
3, rue Joliot Curie, 91192, Gif-sur-Yvette, France.
[2]Faculty of Engineering, University of San Luis Potosí (UASLP), Dr. Manuel Nava 8, Mexico.
[3]Coord. Acad. Región Altiplano, UASLP, Matehuala, S.L.P, Mexico

Corresponding author: C.-F. Méndez-Barrios (e-mail: cerfranfer@gmail.com).

ABSTRACT The results presented in this paper deal with the design of a current sensorless delay–based controller for the closed–loop stabilization of a photovoltaic system under an MPPT scheme using a boost dc/dc converter. Some applications of such topology are dc microgrids, solar vehicles, or stand-alone systems, to mention a few. The basis of this control scheme relies on the feedback linearization control technique coupled with a delay–based low-order controller. In order to study the stability, the proposed approach uses a geometric point of view which allows the partitioning of the controller parameters space into regions with similar stability characteristics (same number of unstable characteristic roots). The most important contribution of the paper relies on providing practical guidelines to tune the gains of the proposed delay–based controller, ensuring asymptotic stability of the closed–loop system and fulfilling the requirements for photovoltaic applications. In addition, the proposed approach allows the design a non-fragile controller with respect to the controller gains. Furthermore, in order to test the effectiveness of the control scheme presented, experimental results evaluating the closed–loop system performance under set-point changes and abrupt irradiance disturbances are addressed using a solar array simulator and a battery bank as load.

INDEX TERMS DC/DC Converter, Delay-Based Controller, Feedback Linearization, MPPT Scheme, PV Systems.

I. INTRODUCTION

RENEWABLE energies have been one of the main areas of interest by governments and organizations of almost all countries, since these type of energy sources are considered the cleanest for the environment. As it has been stated in [25], among the alternatives of renewable energies, photovoltaic (PV) systems has experienced significant growth in recent years, close to 60% in Europe. In fact, as discussed in [8], [15], these systems are being integrated to the electrical grid more commonly than in past years.

Based on the above observations, it becomes evident that higher precision and safety requirements will be demanded by the power grid companies as this tendency continues to expand. In order to provide such features, Power Electronics

(PE) attends directly the high efficiency power conversion problem. In PV systems, it is well known that one of the main solutions to this problem is the application of Maximum Power Point Tracking (MPPT) techniques [5]. In this sense, the most important task relies on the proper control scheme designed to be applied to a PE device.

The main idea behind MPPT techniques consists in finding the Maximum Power Point (MPP) by adjusting the impedance perceived by the Photovoltaic Module (PVM). This process consists in two dependent tasks. First, a control scheme is proposed to regulate the PV voltage at the MPP. Second, an algorithm to compute the optimal reference must be designed. In order to solve such control problems, this work uses a topology based on a boost dc/dc converter. As

TABLE 1. Comparative Table of Control Techniques for PV MPPT Systems Using a Boost dc/dc Converter

References	Number of Sensors in the Control Scheme	Control Strategy	Settling Time	Evaluation Under Transient Conditions
[6]	$2-(v_{pv}, i_{pv})$	Sliding Mode Control	$0.2ms$	✓
[30]	$2-(v_{pv}, i_L)$	Adaptive Control	$14.3ms$	✗
[21]	$3-(v_{pv}, i_{pv}, i_L)$	Double Integral Sliding Mode Control	$150ms$	✗
[10]	$2-(v_{pv}, i_{pv})$	Sliding Mode Control	$0.5ms$	✓
[24]	$3-(v_{pv}, i_{pv}, i_L)$	Adaptive Passivity Based Control	$300ms$	✗
[7]	$4-(v_{pv}, i_{pv}, i_L, v_o)$	Backstepping Sliding Mode Control	$50ms$	✓
[1]	$4-(v_{pv}, i_{pv}, i_L, v_o)$	Sliding Mode Control	$1ms$	✓

a first approach to the development of a MPPT strategy, our main contribution is focused on the PV voltage regulation problem. As discussed in [14], [27], a variety of benefits can be achieved by using MPPT techniques in conjunction with closed–loop control strategies, such as efficiency improvement and low frequency disturbances rejection in the load terminals.

It is worth mentioning that there exist several works that have considered a similar topology but using different control methods. Some of these works are summarized in Table 1. From this table, one can note a variety of control techniques with different needs for its implementation. One may notice the following observations: (i) all solutions require at least two sensors; (ii) moreover, at least a current sensor is needed; (iii) not all solutions are evaluated under transient conditions. By contrast, the delay-based control scheme proposed in this work requires: (i') only one voltage sensor and consequently, (ii') no current sensors are needed; (iii') also, experimental results considering abrupt irradiance disturbances are presented.

Let us emphasize briefly some of the advantages of not requiring a current measurement. One of the main benefits is that current sensors are often large and of expensive implementation in the control system. By contrast, it is worth mentioning that current measurements are commonly available on MPPT systems since such measurements are regularly required in MPPT algorithms such as P&O. However, it is also worth to mention that these can also be avoided by using the fractional method (see, for instance, [16]) and moreover, it can be also estimated; such is the case in [17], in which a model-based predictive control principle is used to predict the states of the PV system.

The method proposed in the sequel is inspired by the ideas developed by the authors in [9], [20] and [31]. On one hand, the work made in [9] proposes the use of a buck dc/dc converter using feedback linearization and a low order controller of PID (Proportional-Integral-Derivative) type. Among low-order controllers, those of PID-type have shown a well-known suitable performance coping with parametrical uncertainties and undesired disturbances, also, to achieve elimination of steady-state errors and transient response manipulation (see, for instance, [3], [22]). However, as reported in [2], [3], one of the main drawbacks of PID controllers is related to the tuning of the derivative action which may amplify additive high-frequency noise in measurements.

On the other hand, in order to circumvent the above mentioned problem, one can notice that the Euler's approach to an approximation of the derivative:

$$y'(t) \approx \frac{y(t) - y(t - h)}{h},$$

for small $h > 0$, suggests to replace the derivative action by using delays [28]. As seen in the sequel, the feedback linearized system using a boost dc/dc converter has a relative degree two, that roughly speaking, consists in a chain of two integrators. Thus, one of the main contributions of this paper is to propose a delay–based control scheme in conjunction with explicit analytical tools that allows designing non-fragile stabilizing controller for these types of systems. In the remaining part of the paper, this scheme will be called Pδ (Proportional-Delayed) controller.

In this vein, a more complex behavior is proposed through the delay–based feedback loop. In contrast with the obtained second order open–loop transfer function, a delayed system has an infinite number of characteristic roots. On one hand, due to the fact that these roots are deeply related to the behavior of the output of the system, we are dealing with a more diverse system in terms of dynamical behavior. On the other hand, this mere fact complicates the overall stability analysis, since the classical Routh-Hurwitz criterion of linear systems is no longer applicable. Nevertheless, as stated in [13], besides the fact that including a delay will induce a more complex behavior, it is important to point out that the delay phenomenon can also promote the system's stability, where classical PID controllers fail to stabilize the closed-loop system.

Encouraged by the previous observations, in this work we propose the use of PIδ controllers instead of standard of PID type in order to achieve two technical objectives. First, as seen in the experimental results section, to decrease the number of sensors needed for the implementation to only one voltage sensor. Second, as mentioned in [12] and references therein, to reduce the processing effort in the application of such controller in comparison to one of PID type. This is due to the fact that delaying a signal is numerically simpler than derivating it, in which some numerical procedure or algorithm is required. Moreover, we propose the adding of an integral action by designing a Proportional-Integral-Delayed (PIδ) controller to achieve steady state error equal to zero in its experimental application and to cope with parametric uncertainties.

The main contributions of this work can be summarized as follows:

C1: We present a control scheme for the proper regulation of the PV voltage of a PVM by using a boost dc/dc converter and a delay–based controller guaranteeing internal stability;

C2: A tunning methodology for a PIδ controller is presented. In fact, this methodology provides necessary and sufficient conditions for the stabilization of the closed-loop system;

C3: The fragility problem of the PIδ controller is studied in terms of the integral and delayed actions;

C4: Experimental tests for this delay–based control scheme are addressed using a 350 W boost dc/dc prototype and a solar array simulator. Particularly, we test the closed-loop scheme under set-point changes and solar irradiation disturbances.

The experimental test bench used for the validation of this control scheme consists in a standalone PV system with a battery bank as load. The main goal is to validate a scenario with a fixed dc bus, in this case emulated by a battery bank. This situation is typicaly founded in stand-alone applications, where a battery bank is used as energy storage when solar irradiation is not available. Moreover, this can be applied in the same manner to an MPPT distributed system in which such voltage output is not fixed. Finally, notice that even without a constant output voltage only voltage sensors are required, and still no current sensors are needed.

The remaining paper is organized as follows: Section II discusses the modeling of the boost dc/dc converter on an MPPT system. Section III describes the control scheme proposed and some important remarks are addressed, such as the stability of the zero dynamics. Section IV concerns to the presentation of the necessary results to develop a stability analysis of such delayed control scheme through a frequency-based approach (see also the ideas proposed by Neimark [19], related to $\mathcal{D}$-partition curves). In addition, this section discusses the fragility problem of the PIδ controller. Section V shows an illustrative example on how such results can be applied in order to tune the PIδ controller. Moreover, several experimental tests using a solar array simulator in order to verify the performance of the control strategy are proposed. Finally, Section VI discusses some concluding remarks on the main results of this work.

II. PV BOOST DC/DC CONVERTER SYSTEM

This section describes the open-loop system considered along this work, as well as some assumptions that will be taken into account in order to perform its closed–loop stability analysis. The methodology presented in the sequel follows similar steps to those proposed in [9], but applied to the analysis of a boost dc/dc converter and using a delay-based controller.

The topology consisting of the equivalent electrical circuit of the boost dc/dc power converter, a PV module and a load element is illustrated in Fig. 1.

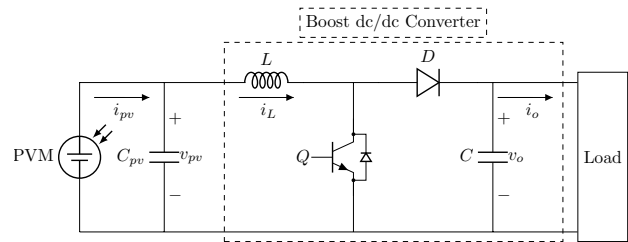From this figure, the average model is described by the

FIGURE 1. MPPT System considering a Boost dc/dc converter.

following equation:

$$\dot{\boldsymbol{x}} = \boldsymbol{f}(\boldsymbol{x}) + \boldsymbol{g}(\boldsymbol{x})u, \quad y = h(\boldsymbol{x}) = x_1, \quad (1)$$

with

$$\boldsymbol{f}(\boldsymbol{x}) := \begin{bmatrix} -\frac{1}{C_{pv}}x_2 + \frac{1}{C_{pv}}i_{pv} \\ \frac{1}{L}x_1 - \frac{1}{L}x_3 \\ \frac{1}{C}x_2 - \frac{1}{C}i_o \end{bmatrix}, \quad \boldsymbol{g}(\boldsymbol{x}) := \begin{bmatrix} 0 \\ \frac{1}{L}x_3 \\ -\frac{1}{C}x_2 \end{bmatrix}, \quad (2)$$

where the state vector is defined by $x = [x_1, x_2, x_3]^T := [v_{pv}, i_L, v_o]^T$, v_{pv} represents the input voltage in the terminals of the capacitor C_{pv}, i_L denotes the current through the inductor L and v_o is the output voltage in terminals of the capacitor C. In addition, i_{pv} denotes the PV current generated by the PV module, i_o is the load current and $u \in [0, 1]$ defines the limited control variable (duty cycle for the switch Q_1).

Remark 1: As mentioned in the introduction, our main goal in the closed–loop scheme, is the proper regulation of the PVM voltage v_{pv}. This constant reference defined as v_{pv}^* is obtained by an external MPP tracking algorithm as shown in Fig. 2. It is worthy of remark that the MPP tracking is by itself a relevant research problem to be considered (see, for instance, [4], [29]), where important phenomena are associated, such as partial shading, mismatch conditions (due to the interconnection of solar cells or modules with different properties), just to mention a few. In this vein, this work will focus on the regulation problem.
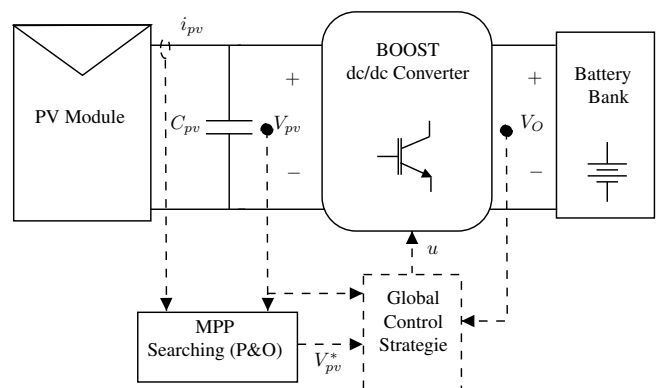

FIGURE 2. MPPT System Schematic.

In the remaining part of the paper, we consider the following assumptions:

Assumption 1: The voltage reference v_{pv}^* is considered as a piecewise constant signal.

Assumption 2: The current i_{pv} is considered as a very low–frequency signal.

Assumption 3: The inductance value of the boost converter is as low as possible, i.e., $0 < L \ll 1$.

The ideal voltage reference v_{pv}^* is located at the maximum power point v_{mpp}. We consider Assumption 1 since the MPP is a slow time–varying signal which mainly changes by effects of the ambient temperature. In a similar manner, we consider Assumption 2 since, ideally, i_{pv} must be of a direct current type and it changes with respect to solar irradiation disturbances. Finally, as can be seen in the sequel, Assumption 3 is nothing else than a design consideration helpful for the control scheme design. Furthermore, as can be seen from (1), the input capacitor voltage v_{pv} is chosen as the output of the system. It is worth mentioning that similar assumptions have been considered in [9] and [31].

III. GLOBAL CONTROL STRATEGY

This section presents the proposed control scheme for the regulation problem of the PV system. The procedure consists in two basic steps. First, a feedback linearization control scheme is designed to obtain an input-output linear mapping. Second, we propose a delayed controller in order to stabilize the resulting dynamics.

By computing the derivatives of the output $y = x_1$, the following set of equations are derived:

$$C_{pv}\dot{y} = -x_2 + i_{pv}, \tag{3}$$

$$LC_{pv}\ddot{y} = -x_1 + x_3 - x_3 u + L\frac{d}{dt}(i_{pv}). \tag{4}$$

Since the control signal u appears up to the second derivative, the system has a relative degree $\rho = 2$ in an open and not connected set $\beta = \{x \in \mathbb{R}^3 \,|\, x_3 \neq 0\}$. Thus, by considering Assumption 2 into (4) we obtain:

$$u = \left(1 - \frac{x_1}{x_3}\right) - \frac{1}{x_3}v, \tag{5}$$

which reduces the input-output mapping to:

$$LC_{pv}\ddot{y} = v, \tag{6}$$

where v is considered as an auxiliary control law.

A. PIδ CONTROL STRATEGY

As mentioned in the Introduction, the main focus of this work concerns the design of a PIδ controller for the regulation of the output of system (6). In this vein, considering the constant voltage reference v_{pv}^*, we propose the following auxiliary control law as:

$$v(t) = k_p\left(v_{pv}^* - y(t)\right) + k_\delta\left(v_{pv}^* - y(t-\tau)\right) + k_i\int_0^t \left(v_{pv}^* - y(s)\right)ds. \tag{7}$$

Hence, we can rewrite the system (6) in terms of the output error $e(t) := y(t) - v_{pv}^*$, as follows:

$$LC_{pv}\ddot{e}(t) + k_i\int_0^t e(s)ds + k_p e(t) + k_\delta e(t-\tau) = 0, \tag{8}$$

where τ is a fixed delay value. It is worth mentioning that the form of the system (6) suggests the use of a proportional-derivative controller to achieve asymptotic stabilization. Nevertheless, as we will detail in Section IV, the delay-based controller can asymptotically stabilize the closed-loop system by a proper choice of the controller parameters (k_p, k_δ, τ). This implies that as $t \to \infty$, then, $e(t) \to 0$ and therefore $y \to v_{pv}^*$. In addition, in order to improve the system's performance, we have included the integral term in (7) with the aim to cope with the parametric uncertainties. The analytical procedure to tuning such a PIδ−controller $(k_p, k_i, k_\delta, \tau)$ will be explained in detail in the Section IV.

B. ZERO DYNAMICS

As mentioned previously, the system (1) has a relative degree $\rho = 2$. As it is well known in the literature (see, for instance [26]), there exists a zero dynamics which has to be properly analyzed in order to be able to consider the linear mapping (6). This section covers in detail the characterization of such dynamics.

First, as mentioned in [26], we need to find a diffeomorfism, also described as the change of coordinates:

$$z = \begin{bmatrix} \epsilon_1 \\ \epsilon_2 \\ \eta \end{bmatrix} = T(x) = \begin{bmatrix} h(x) \\ \langle \nabla h, f \rangle \\ \varphi(x) \end{bmatrix}, \tag{9}$$

with inverse:

$$x = T^{-1}(z). \tag{10}$$

Next, in order to express the dynamics of the change of coordinates (9) in the normal form, the function $\varphi(x)$ must satisfy the following condition:

$$\langle \nabla\varphi, g \rangle = 0. \tag{11}$$

Hence, following (11) we get:

$$Cx_3\frac{\partial\varphi}{\partial x_2} = Lx_2\frac{\partial\varphi}{\partial x_3}. \tag{12}$$

It is clear to see, that a solution of the partial differential equation (12) can be easily computed by assuming a solution φ satisfying:

$$\frac{\partial\varphi}{\partial x_2} = 2Lx_2, \quad \frac{\partial\varphi}{\partial x_3} = 2Cx_3. \tag{13}$$

The above consideration leads to the solution:

$$\varphi(x) = Lx_2^2 + Cx_3^2. \tag{14}$$

Hence, this diffeomorfism and its inverse are given by:

$$z = T(x) = \begin{bmatrix} x_1 \\ -\frac{1}{C_{pv}}x_2 + \frac{1}{C_{pv}}i_{pv} \\ Lx_2^2 + Cx_3^2 \end{bmatrix}, \tag{15}$$

$$\boldsymbol{x} = \boldsymbol{T}^{-1}(\boldsymbol{z}) = \begin{bmatrix} \epsilon_1 \\ -C_{pv}\epsilon_2 + i_{pv} \\ \sqrt{\frac{1}{C}\left(\eta - L\left(C_{pv}\epsilon_2 - i_{pv}\right)^2\right)} \end{bmatrix}. \quad (16)$$

Now, in order to model a battery bank as load, let us consider $i_o = \gamma(x_3)$, where γ has the property that $\text{sgn}(\gamma) = \text{sgn}(x_3)$ for all $x_3 \in \mathbb{R}$. Let $\boldsymbol{\epsilon} := [\epsilon_1, \epsilon_2]^T$, by computing the time derivative of $\boldsymbol{z}$ and considering (6) and (15), the dynamics of $\boldsymbol{z}$ can be split into a linear system:

$$\dot{\boldsymbol{\epsilon}} = \begin{bmatrix} 0 & 1 \\ 0 & 0 \end{bmatrix}\boldsymbol{\epsilon} + \begin{bmatrix} 0 \\ 1 \end{bmatrix}\frac{1}{LC_{pv}}v \quad (17)$$

in conjunction with a nonlinear one:

$$\dot{\eta} = -2\gamma(x_3(\eta))x_3(\eta) + 2\epsilon_1(C_{pv}\epsilon_2 - i_{pv}). \quad (18)$$

Finally, in order to characterize the zero dynamics of the system we assume that as $t \to \infty$, then $\boldsymbol{\epsilon} \to [0, 0]^T$ and:

$$x_3(\eta) \to \sqrt{\frac{1}{C}\eta - \frac{L}{C}i_{pv}^2}. \quad (19)$$

Considering the above results, the zero dynamics of the system is given as:

$$\dot{\eta} = -2\gamma(x_3(\eta))x_3(\eta). \quad (20)$$

In order to verify the stability of such dynamics, we propose the classical Lyapunov function:

$$\mathcal{V}(\eta) := \frac{1}{2}\eta^2. \quad (21)$$

Computing its time derivative yields:

$$\dot{\mathcal{V}} = -2\gamma(x_3(\eta))x_3(\eta)\eta. \quad (22)$$

Now, according to (14) and (19) we observe that $\eta \geq 0$ and $x_3(\eta) \geq 0$, respectively. Hence, $\gamma \geq 0$ implying that $\dot{\mathcal{V}} \leq 0$. This last condition allows concluding the stability of the zero dynamics.

IV. PIδ CONTROLLER DESIGN

As mentioned above, the proposed auxiliary control law consists in the use of a PIδ controller. The most important contribution of this paper lies in the development of the necessary tools to implement an appropriate tunning of the controller parameters (k_p, k_i, k_δ) with a delay value τ.

The proposed approach relies in two steps. First, assuming $k_i = 0$ we aim to find at least one stability region in the parameters space (k_p, k_δ) with a fixed delay value τ. Second, in order to tune the integral gain k_i, we take into account a stabilizing controller pair (k_p^*, k_δ^*), and we establish a similar method to find a stability region on the parameters space (k_δ, k_i). Such a procedure will be explained in detail in the sequel.

Consider the system (6) together with the proposed control law (7). Hence, the closed–loop transfer function of the linearized system is given as:

$$G_{cl}(s) = \frac{(k_p + k_\delta e^{-\tau s})s + k_i}{LC_{pv}s^3 + (k_p + k_\delta e^{-\tau s})s + k_i}. \quad (23)$$

Thus, the closed–loop characteristic equation is given by the following quasi-polynomial:

$$\tilde{\Delta}(s; k_p, k_\delta, k_i, \tau) = LC_{pv}s^3 + (k_p + k_\delta e^{-\tau s})s + k_i = 0. \quad (24)$$

Notice that by considering only a proportional-delay controller (i.e., $k_i = 0$) in (23) the characteristic equation behaves as:

$$\Delta(s; k_p, k_\delta\tau) = LC_{pv}s^2 + k_p + k_\delta e^{-\tau s} = 0. \quad (25)$$

Remark 2: It is well known that the stability of a linear system free of delay, is directly related to the location of the roots of its characteristic equation. More precisely, the system is asymptotically stable, if and only if, all roots of its characteristic equation lie on the left-half plane of the complex plane. This argument is also true for delayed linear systems (see, for instance, [18]). However, unlike the free delay case, in time-delay systems, it is well known that the quasi-polynomial (25) (or (24)) has an infinite number of roots that depend continuously on the parameter (k_p, k_δ, τ) (or $(k_p, k_\delta, k_i, \tau)$). Hence, the corresponding closed-loop system will be asymptotically stable if and only if the rightmost characteristic root is located in $\mathbb{C}_-$.

A. STABILITY CROSSING CURVES CHARACTERIZATION

Now, with the purpose of developing a stability analysis, we first derive the stability crossing boundaries. In other words, we characterize the controller parameters choice (k_p, k_δ, k_i) such that the quasi-polynomial (25) has at least one root on the imaginary axis (at $s = \pm j\omega$) of the complex plane. In order to introduce formally such ideas, consider the following definitions.

Definition 1 (Frequency crossing set): The frequency crossing set $\Omega \in \mathbb{R}$ is the set of all ω such that, there exists a parameters choice $(k_p, k_i, k_\delta, \tau)$ (or (k_p, k_δ, τ)) such that:

$$\tilde{\Delta}(j\omega; k_p, k_i, k_\delta, \tau) = 0. \quad (26)$$

Remark 3: Taking the complex conjugate of (26), the following is true:

$$\tilde{\Delta}(-j\omega; k_p, k_i, k_\delta, \tau) = \overline{\tilde{\Delta}(j\omega; k_p, k_i, k_\delta, \tau)}.$$

Therefore, in the sequel only nonnegative frequencies are considered, i.e., $\Omega \subset \mathbb{R}_+ \cup \{0\}$.

Definition 2 (Stability Crossing Curves): The stability crossing curves $\mathcal{T}$ is the set of all parameters $(k_p, k_i, k_\delta, \tau) \in \mathbb{R}^3 \times \mathbb{R}_+$ for which there exists at least one $\omega \in \mathbb{R}_+ \cup \{0\}$ such that $\tilde{\Delta}(j\omega; k_p, k_i, k_\delta, \tau) = 0$. For a fixed delay value $\tau^* \in \mathbb{R}_+$, any point $\boldsymbol{k} \in \mathcal{T}$ is known as a crossing point.

Remark 4: For analysis purpose, in some situations we consider τ^* as a fixed parameter. In such cases $\mathcal{T}$ will be composed by the parameters $(k_p, k_i, k_\delta, \tau^*) \in \mathbb{R}^3 \times \mathbb{R}_+$ satisfying Definition 2. Similar definitions hold for Δ, i.e., for the $P\delta-$controller.

Proposition 1: Let $\tau \in \mathbb{R}_+$ be a fixed delay value. Then, the characteristic equation of the closed–loop system Δ has at

least one pair of roots on the imaginary axis (at $s = \pm j\omega$), if and only if the controller gains $\boldsymbol{k}(\omega) := [k_p, k_\delta]^T$, are given as:

$$k_\delta = (-1)^n \left(-k_p + \frac{LC_{pv}\pi^2}{\tau^2} n^2 \right), \quad \text{for } \omega = \frac{n\pi}{\tau}, \quad (27)$$

$$k_p = LC_{pv}\omega^2 \quad \& \quad k_\delta = 0, \quad \text{for } \omega \in \left(\frac{(n-1)\pi}{\tau}, \frac{n\pi}{\tau} \right), (28)$$

for all $n \in \mathbb{Z}_+$. Furthermore, it has a single root at the origin ($\omega = 0$) if and only if:

$$k_\delta = -k_p \quad \text{and} \quad k_p \neq 0. \quad (29)$$

Proof 1: As a first step let us consider the characteristic equation (25) at $s = j\omega$, yielding to

$$-LC_{pv}\omega^2 + k_p + k_\delta \cos(\tau\omega) - jk_\delta \sin(\tau\omega) = 0. \quad (30)$$

Clearly (30) holds whenever $n \in \mathbb{Z}$ and $\omega = \frac{n\pi}{\tau}$, or when $k_\delta \equiv 0$. Thus, considering such situations in (30) we derive (27) and (28), respectively. Finally, by setting $s = 0$ in (30) and following similar arguments than those presented above, leads to (29).

Remark 5: It is clear to see from the structure of Δ or $\tilde{\Delta}$, that in the absence of the delay term, the closed-loop system will be oscillatory (if $k_p > 0$) or even unstable (if $k_p < 0$). Such an observation is congruent with the derived experimental results (see, for instance, the behavior of controller c_3, in section V-B).

Proposition 2: Let $\tau \in \mathbb{R}_+$ and $k_p^* \in \mathbb{R}$ be fixed values. The characteristic equation of the closed–loop system has a pair of roots on the imaginary axis ($s = j\omega$), if and only if the controller gains $\tilde{k}(\omega) = [\tilde{k}_\delta(\omega), \tilde{k}_i(\omega)]^T$, are given as:

$$\tilde{k}_\delta(\omega) = \frac{LC_{pv}\omega^2 - k_p^*}{\cos(\tau\omega)}, \quad (31)$$

$$\tilde{k}_i(\omega) = -\omega \tan(\tau\omega)(LC_{pv}\omega^2 - k_p^*), \quad (32)$$

for all $\omega \in \mathbb{R}_+$ such that $\omega \neq \frac{(2n+1)\pi}{2\tau}$ with $n \in \mathbb{Z}_+ \cup \{0\}$. Furthermore, it has a single root at the origin ($\omega = 0$) iff:

$$k_i = 0 \quad \text{and} \quad k_\delta \neq -k_p^*. \quad (33)$$

Proof 2: Consider the characteristic equation (24) with $s = j\omega$,

$$(k_\delta\omega \sin(\tau\omega) + k_i) + j \left(k_\delta\omega \cos(\tau\omega) + k_p^*\omega - LC_{pv}\omega^3 \right) = 0. \quad (34)$$

It is clear to see that (34) is fulfilled, as long as the following equation holds:

$$\begin{bmatrix} \omega \sin(\tau\omega) & 1 \\ \omega \cos(\tau\omega) & 0 \end{bmatrix} \begin{bmatrix} k_\delta \\ k_i \end{bmatrix} = \begin{bmatrix} 0 \\ LC_{pv}\omega^3 - k_p^*\omega \end{bmatrix}.$$

Thus, assuming that $\omega \neq \frac{(2n+1)\pi}{2\tau}$, $\forall n \in \mathbb{Z}_+ \cup \{0\}$ we derive (31) and (32). In a similar way, by setting $s = 0$ in $\tilde{\Delta}$ leads to (33).

Based on the previous results, for a fixed delay value $\tau^* \in \mathbb{R}_+$ the stability crossing curves for a $P\delta$ controller

$\boldsymbol{k} = [k_p, k_\delta]^T$ are characterized by means of the following manifolds:

$$\mathcal{T}_n^\ell := \left\{ \boldsymbol{k} \in \mathbb{R}^2 \,\middle|\, k_\delta = (-1)^n \left(-k_p + \frac{LC_{pv}\pi^2}{\tau^2} n^2 \right) \right\},$$

$$\mathcal{T}_n^p := \left\{ \boldsymbol{k} \in \mathbb{R}^2 \,\middle|\, \boldsymbol{k} = \left[LC_{pv}\omega^2, 0 \right]^T, \omega \in \left(\frac{\pi}{\tau}(n-1), \frac{\pi}{\tau}n \right) \right\},$$

where $n \in \mathbb{Z}_+$. The curve characterizing a real simple crossing is given by:

$$\mathcal{T}_o := \left\{ \boldsymbol{k} \in \mathbb{R}^2 \,|\, k_\delta + k_p = 0 \text{ and } k_p \neq 0 \right\}.$$

For the PIδ controller, consider $\tilde{\boldsymbol{k}} := [k_\delta, k_i]^T$ and let $\tau^* \in \mathbb{R}_+$ and $k_p^* \in \mathbb{R}$ be fixed values. Then, the stability crossing curves are defined as:

$$\widetilde{\mathcal{T}}_n^m := \left\{ \tilde{\boldsymbol{k}} \in \mathbb{R}^2 \,\middle|\, \tilde{\boldsymbol{k}} = \tilde{\boldsymbol{k}}(\omega), \omega \in \left(\frac{(\text{sgn } n)(2n-1)\pi}{2\tau}, \frac{(2n+1)\pi}{2\tau} \right) \right\},$$

for $n \in \mathbb{Z}_+ \cup \{0\}$, and the curve characterizing a real simple crossing is given by

$$\widetilde{\mathcal{T}}_o := \left\{ \tilde{\boldsymbol{k}} \in \mathbb{R}^2 \,\middle|\, k_i = 0 \text{ and } k_\delta \neq -k_p^* \right\}. \quad (35)$$

Thus, the stability crossing curves can be described as

$$\mathcal{T} = \bigcup_n \mathcal{T}_n^\ell \bigcup_n \mathcal{T}_n^p \bigcup \mathcal{T}_o, \quad (36)$$

$$\widetilde{\mathcal{T}} = \bigcup_n \widetilde{\mathcal{T}}_n^m \bigcup \widetilde{\mathcal{T}}_o, \quad (37)$$

for the Pδ and PIδ controllers, respectively.

B. CROSSING DIRECTIONS

In order to compute a stability index, which is the number of roots in the RHP for a given parametrical region, it is of interest to characterize the behavior of the roots as a function of the corresponding parameter, when a parameter deviates from any boundary. The following results are the main tools to achieve such a task.

Proposition 3: Let $\tau \in \mathbb{R}_+$ be a fixed delay value. Then, as $\boldsymbol{k}$ crosses in any direction from left to right of: $\mathcal{T}_n^\ell$, $n \in \mathbb{Z}_+$ traversing the point $\hat{\boldsymbol{k}} = [\hat{k}_p, \hat{k}_\delta]^T \in \mathcal{T}_n^\ell$, one pair of roots of the characteristic equation (25) moves from the LHP to the RHP of the complex plane if $\hat{\boldsymbol{k}}$ satisfies the following conditions:

$$\hat{k}_\delta > 0 \text{ for } n \text{ even}, \quad \hat{k}_\delta < 0 \text{ for } n \text{ odd}. \quad (38)$$

Furthermore, the crossing of the roots is from the RHP to the LHP if these inequalities are reversed.

Proof 3: Consider the characteristic equation (25). Now, by the Implicit Function Theorem (see, for instance, [11]), we have:

$$\frac{ds}{dk_p} = -\frac{\frac{\partial\Delta}{\partial k_p}}{\frac{\partial\Delta}{\partial s}}, \qquad \frac{ds}{dk_\delta} = -\frac{\frac{\partial\Delta}{\partial k_\delta}}{\frac{\partial\Delta}{\partial s}}, \quad (39)$$

where:

$$\frac{\partial\Delta}{\partial s} = 2LC_{pv}s - \tau k_\delta e^{-\tau s}, \quad (40)$$

$$\frac{\partial\Delta}{\partial k_p} = 1, \quad \frac{\partial\Delta}{\partial k_\delta} = e^{-\tau s}. \quad (41)$$

IEEE Access

Then, by taking $s = jn\frac{\pi}{\tau}$, for $n \in \mathbb{Z}_+$ yields

$$\left[\frac{ds}{dk_p}\right]^{-1}\Bigg|_{s=j\frac{n\pi}{\tau}} = \tau k_\delta(-1)^n - j\frac{2\pi n LC_{pv}}{\tau}. \quad (42)$$

Since, $\tau \in \mathbb{R}_+$ and $\frac{ds}{dk_\delta} = \frac{ds}{dk_p}e^{-\tau s}$, we can conclude:

$$\text{sgn}\left\{\Re\left\{\frac{ds}{dk_p}\Bigg|_{s=j\frac{n\pi}{\tau}}\right\}\right\} = \text{sgn}\left\{(-1)^n k_\delta\right\}. \quad (43)$$

$$\text{sgn}\left\{\Re\left\{\frac{ds}{dk_\delta}\Bigg|_{s=j\frac{n\pi}{\tau}}\right\}\right\} = \text{sgn}\left\{k_\delta\right\}. \quad (44)$$

Therefore, the proof follows straightforwardly by simply observing that (43)-(44) imply (38).

Proposition 4: Let $\tau \in \mathbb{R}_+$ be a fixed delay value. Then, one pair of roots of the characteristic equation (25) moves from the LHP to the RHP of the complex plane as $\boldsymbol{k}$ crosses the curve $\mathcal{T}_n^p$ in the increasing direction of k_δ if n is odd. Furthermore, the crossing is from the RHP to the LHP if n is even.

Proof 4: Consider the characteristic equation (25). Making use of the Implicit Function Theorem and following similar arguments than those presented in the proof of Proposition 3, one gets:

$$\left[\frac{ds}{dk_\delta}\right]^{-1} = \tau k_\delta - 2LC_{pv}se^{\tau s}. \quad (45)$$

Now, by considering the set of stability crossing curves $\mathcal{T}_n^p$, $s = j\omega$ for $\omega \in \mathcal{I}_n := \left(\frac{\pi}{\tau}(n-1), \frac{\pi}{\tau}n\right)$ and $\boldsymbol{k} = \left[LC_{pv}\omega^2, 0\right]^T$, yields

$$\mathcal{D}(\omega) := \Re\left\{\left[\frac{ds}{dk_\delta}\right]^{-1}\right\} = 2LC_{pv}\omega\sin(\tau\omega). \quad (46)$$

The proof ends by noting that $\mathcal{D} > 0$ for all $\omega \in \mathcal{I}_n$ with n odd and $\mathcal{D} < 0$ for all $\omega \in \mathcal{I}_n$ with n even.

Proposition 5: Let $\tau \in \mathbb{R}_+$. Then, a simple root of the characteristic equation (25) moves from the LHP to the RHP through the origin as $\boldsymbol{k}$ crosses from left to right the stability crossing curve $\mathcal{T}_o$ if $k_\delta > 0$. Furthermore, the crossing is from the RHP to the LHP if the inequality is reversed.

Proof 5: By setting $s = 0$, the proof follows the same lines as the proof of Proposition 3.

Proposition 6: Let $\tau \in \mathbb{R}_+$ and k_p^* be fixed values. Then, a simple root of the characteristic equation (24) moves from the LHP to the RHP through the origin as $\tilde{\boldsymbol{k}}$ crosses the k_δ-axis in the increasing direction of k_i if $k_\delta < -k_p^*$. Furthermore, the crossing is from the RHP to the LHP if the inequality is reversed.

Proof 6: The proof follows similar ideas to those presented in the proof of Proposition 3 but setting $s = 0$ and computing $\frac{ds}{dk_i}$.

C. FRAGILITY

In this section we propose an auxiliary result to deal with the fragility problem of a given controller. This result allows evaluating the robustness of a stabilizing controller against parametric uncertainties. Such a measure will become extremely useful when the controller is implemented digitally since there is always a natural uncertainty in the controller parameters due to the finite word length and to rounding errors in numerical computations. Thus, the fragility measure is a desirable parameter to be considered in the design procedure. In this work, we focus exclusively on the delayed and integral action, that is, in the proper tuning of the gains k_δ and k_i by considering the proportional gain k_p and the delay time value τ as fixed parameters.

Consider now the fragility problem, which consists of computing the maximum controller parameters deviation d of a given stabilizing controller $\bar{\boldsymbol{k}} = [\bar{k}_\delta, \bar{k}_i]^T$, such that the closed-loop system remains stable. More precisely, such that the controller gains pair $\bar{k}$ satisfy the following inequality:

$$\sqrt{(k_\delta - \bar{k}_\delta)^2 + (k_i - \bar{k}_i)^2} < d. \quad (47)$$

In order to address this problem, let $\tilde{\boldsymbol{k}}(\omega) = [\tilde{k}_\delta(\omega), \tilde{k}_i(\omega)]^T$ as given in Proposition 2. Bearing in mind this notation, we have the following:

Proposition 7: Let $\tau \in \mathbb{R}_+$ and $k_p^* \in \mathbb{R}$ be fixed values and $\bar{k}$ be a stabilizing controller. Then, the maximum parameter deviation d of $\bar{k}$, such that the closed-loop system remains stable, is given by:

$$d := \min_{\omega \in \Omega_f}\left\{\left\|\tilde{\boldsymbol{k}}(\omega) - \bar{\boldsymbol{k}}\right\|, |\bar{k}_i|\right\}, \quad (48)$$

where the set Ω_f is defined as

$$\Omega_f := \left\{\omega \in \Omega \,\bigg|\, \left\langle\frac{d}{d\omega}\tilde{\boldsymbol{k}}(\omega), \tilde{\boldsymbol{k}}(\omega) - \bar{\boldsymbol{k}}\right\rangle = 0\right\}, \quad (49)$$

where $\langle\cdot,\cdot\rangle$ stands for the inner product.

Proof 7: Assuming that $\bar{k}$ is a stabilizing choice of parameters, then, this is located inside a stability region defined by some appropriate stability crossing boundaries. Therefore, the closed-loop system losses stability if the controller's parametrical choice $\bar{k}$ continuously variates in such a way that it crosses for at least one of its boundaries. Therefore, it is of interest to compute the minimal distance between $\bar{k}$ and the different stability crossing curves.

First, to compute such distance for $\omega \neq 0$, it is necessary to identify the points $\tilde{\boldsymbol{k}}(\omega)$ at which the tangent vectors to this curve are orthogonal to $\tilde{\boldsymbol{k}}(\omega) - \bar{k}$. It is clear to see, that such points must satisfy the following equality

$$\left\langle\frac{d}{d\omega}\tilde{\boldsymbol{k}}(\omega), \tilde{\boldsymbol{k}}(\omega) - \bar{\boldsymbol{k}}\right\rangle = 0.$$

Second, since boundaries are needed, we must consider the distance to $\widetilde{\mathcal{T}}_o$, which is given directly by the magnitude of $|\bar{k}_i|$. Therefore, the proof concludes by taking the minimum of these values, i.e., d is given by (48).
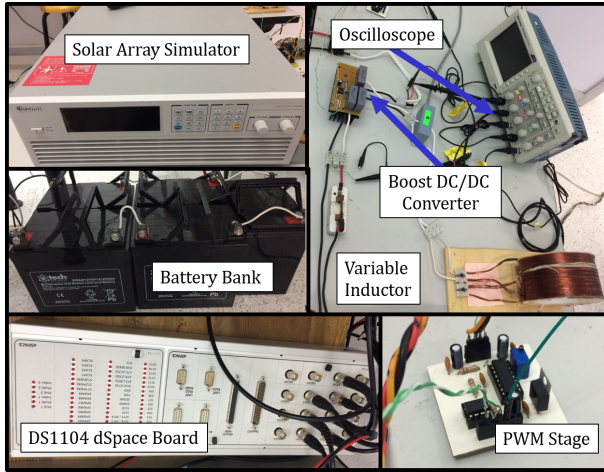
FIGURE 3. Experimental Test Bench - Main Components.

TABLE 2. Passive Elements of the Boost dc/dc Converter

Parameters	Value	Units
C_{pv}	352×10^{-6}	F
L	4.77×10^{-3}	H
C	144×10^{-6}	F

V. EXPERIMENTAL RESULTS

This section presents the application of the previous results to the experimental test bench depicted in Figure 3. More precisely, the design of a stabilizing controller for the PV boost dc/dc converter system. First, by means of the stability crossing curves, the tuning methodology of the PI$\delta-$controller is presented. Second, several experimental results have been taken into consideration in order to evaluate the performance of the control strategy. The standalone PV system consists of a boost dc/dc converter, five $12\,$V lead-acid batteries with a capacity of 80 Ah as load and a solar array simulator as PVM. A series connection has been considered for the battery bank which establishes a dc bus voltage of $60\,$V. The parameters values of the passive elements of the boost dc/dc converter are summarized in Table 2. These values were chosen by considering a continuous mode operation at a rated power of $350\,$W and the power converter PWM stage operating at a switching frequency of $f_c = 10\,$KHz (see, for instance, [23]). The control algorithm was implemented on a DS1104 dSpace board at sampling frequency $f_s = 40\,$KHz. However, the measurements presented in this section were obtained using the following Tektronix equipment: an ac/dc current probe (A622), a high voltage differential probe (P5200) and a digital signal oscilloscope TDS2024B. Finally, the active elements, the power diode D and the power switch Q are STTH30R04W and IRFP250N, respectively. The main components are illustrated in Fig. 3.

A. TUNING METHODOLOGY OF THE PIδ CONTROLLER

Let us consider the system (17) in closed-loop with the $P\delta-$controller, where the fixed delay value has been chosen equal to $\tau = 2 \times 10^{-3}s$. By means of Proposition 1, we construct the stability crossing curves depicted in Fig. 4.
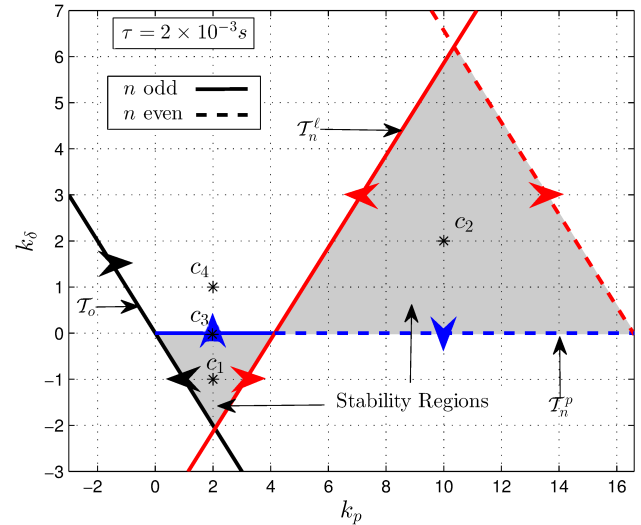

FIGURE 4. $k_p - k_\delta$ Parameters Space Analysis.

In addition, also in this figure for each stability boundary, the crossing directions for which at least a root moves from the LHP to the RHP are indicated by arrows. These crossing directions are derived by applying Propositions 3, 4 and 5. Using the crossing directions of $\mathcal{T}_n^p$ presented in Proposition 3, we can find easily the segments at which the roots will cross to the LHP. Giving as a result the two stability regions illustrated in Fig. 4.

As a next step, let us consider the tuning of the k_i term. To this end, let us consider first the stabilizing P$\delta-$controller c_1, where $(k_p, k_\delta) = (2, -1)$. Then, taking $k_p^* = 2$ in Proposition 2 yields the stability crossing curves depicted in Fig.5.

As in the previous step, by means of Proposition 6 we compute the crossing directions, allowing us to derive the stability region illustrated in Fig. 5. Moreover, the fragility of the stabilizing controller c_1 is analyzed. Using Proposition 7 we compute the maximum deviation allowed, such that the controller c_1 remains stable. The results are summarized in Table 3 and illustrated in Fig. 5.

TABLE 3. Fragility Analysis of Controller c_1 for $\tau = 2 \times 10^{-3}$.

k_p	k_i	k_δ	ω	$|\bar{k}_i|$	d
2	500	-1	1.214×10^3	500	0.137

B. EXPERIMENTAL TESTS

For the experimental tests, the characteristic current-voltage curve set in the solar array simulator was programmed with
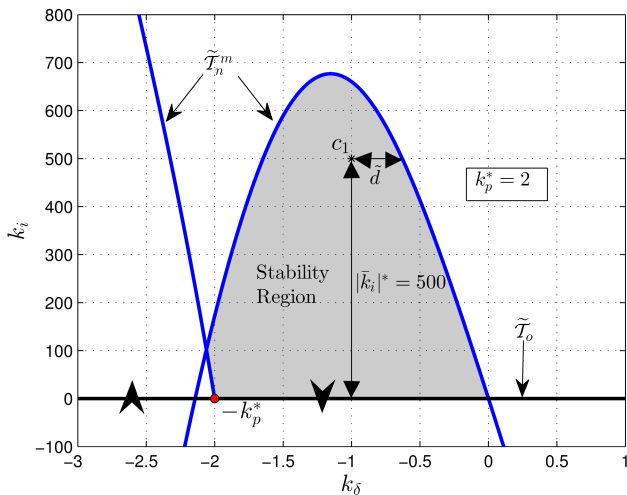
IEEE *Access*

FIGURE 5. $k_\delta - k_i$ Parameters Space Analysis.
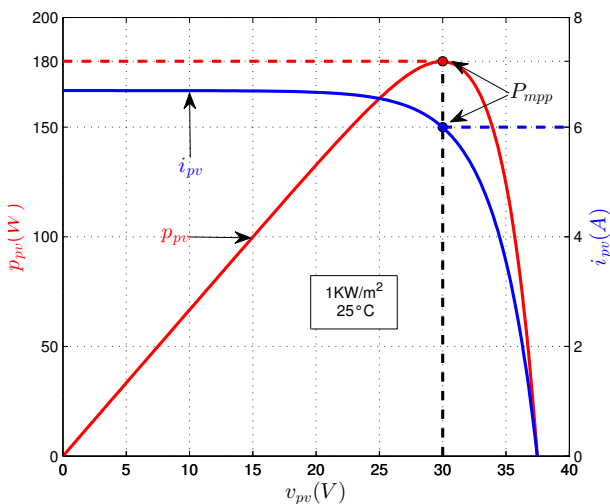

FIGURE 6. Characteristic Current-Voltage Curve Set in the Solar Array Simulator.

180 W in standard conditions as can be appreciated from Fig. 6. From this figure, it is worth to notice that the MPP is located at $v_{mpp} = 30$ V, $i_{mpp} = 6$ A and $P_{mpp} = 180$ W. As mentioned in the test bench description, we consider a battery bank as load of the MPPT system. This common scenario is known as an isolated PV system, at which the main goal is to keep the battery bank completely charged using the energy gathered by the PV modules. Observe that since the auxiliary control law v only needs the PV voltage $x_1 = v_{pv}$, one may notice that the total control law (5) will also require the output voltage $x_3 = v_o$. However, in this experimental results we consider this as a constant voltage of $60V$ since in general this will be the common case. It is worth mentioning that even though this voltage is varying slowly as batteries are being charged, for control purposes, such a voltage can be considered as constant. This, since the numerical uncertainties will be coped by means of the

integral action. In conclusion, for the experiments presented in this section only the PV voltage v_{pv} sensor was needed. Based on the stability regions presented in Fig. 4, we consider the four different controllers summarized in Table 4 and illustrated in Fig. 4.

TABLE 4. PIδ Controllers Parameters

| c_i	k_p	k_i	k_δ	τ [s]
c_1	2	500	-1	2×10^{-3}
c_2	10	600	2	2×10^{-3}
c_3	2	500	0	2×10^{-3}
c_4	2	500	1	2×10^{-3}

Moreover, from figure 4, it is easy to see that two of these controllers are stabilizing controllers (c_1, c_2), whereas the others are not (c_3, c_4). It is worth to mention that the integral term of each stabilizing controller is designed individually following the procedure presented above. Furthermore, the unstable ones are just a variation of c_1 in which the gain related to the delayed action is perturbed.

Now, in order to test the performance of the controllers c_1 and c_2, the following two scenarios are taken into consideration: 1 V and 5 V set-point changes. In this vein, one of the most common MPPT techniques "perturb and observe" (P&O) consists in varying the PV voltage reference in consistent steps changes, by observing the PV power in order to locate the MPP. These tests are designed to analyze the closed-loop system reliance on an online MPPT tracking system that attends such behavior.

The results are summarized in Figs. 7 and 8, where from these figures we can notice that there always exists an abrupt transitory state in which the settling time measured goes from 9 ms to 10.9 ms, where these experiments have been implemented for 1 V and 5 V set-point changes.

Furthermore, it is shown in every test that the control effort remains in the operation interval $u \in [0, 1]$ with this delayed strategy, even for the 5 V set-point changes. This is the ideal scenario in which the closed-loop system must remain. Now, from the comparative table shown in the introduction (Table 1), we can observe that the settling times documented for these experiments goes from 0.2 ms to 300 ms. In addition, we would like to highlight the fact that all these strategies needs at least two sensors, while as discussed above, in the experimental test bench shown in this work, only the PV voltage sensor is required.

As a second experimental test, let us evaluate the system under transient conditions. To this end, the test consists in setting a constant voltage reference $v_{pv}^* = 30$ V, while an irradiance disturbance which oscillates from 100 W/m² to 1000 W/m² is applied by the solar array simulator. We consider this as an abrupt scenario, irradiance variation through the day or even shading caused by clouds movement can be considered as slower scenarios which would be easier to handle for the control system. The obtained results are shown in Fig. 9 for the controllers c_1 and c_2. Moreover, from these
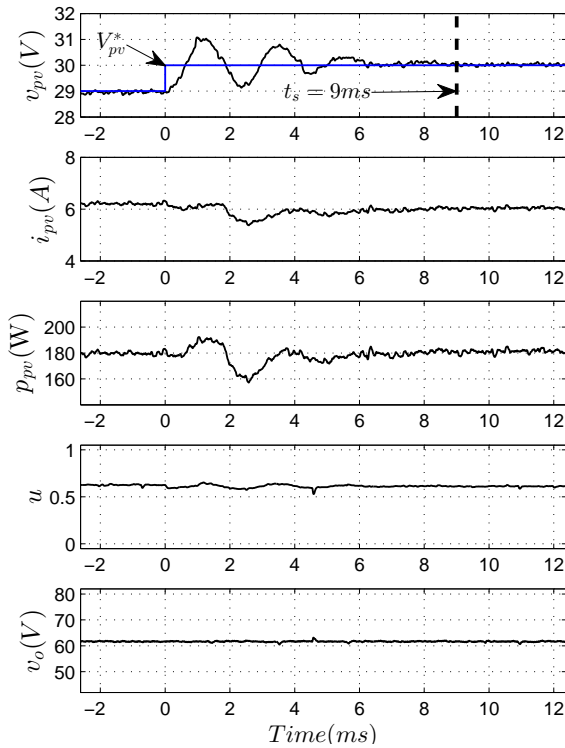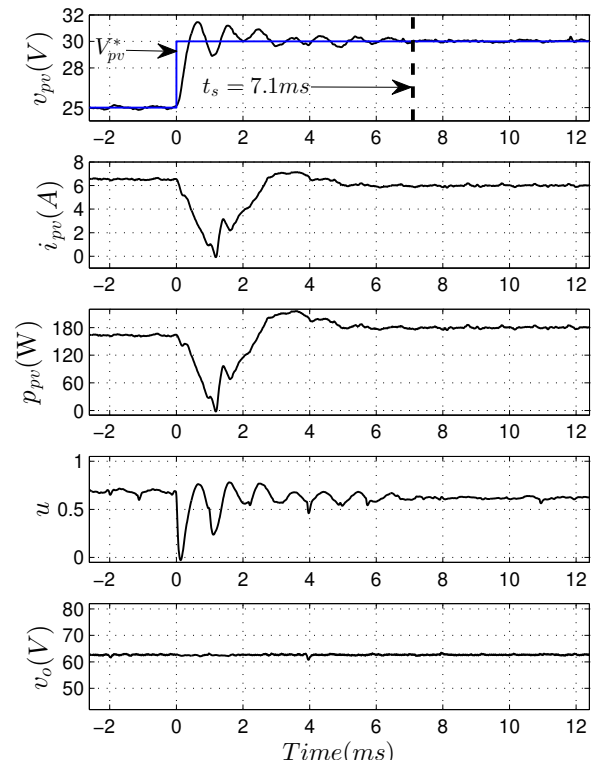
(a) 1 V Variation - Controller c_1
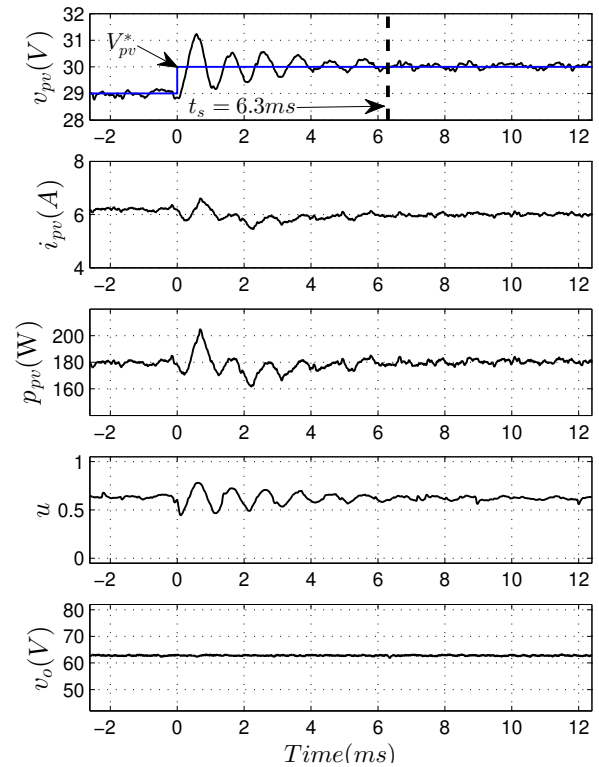
(a) 1 V Variation - Controller c_2
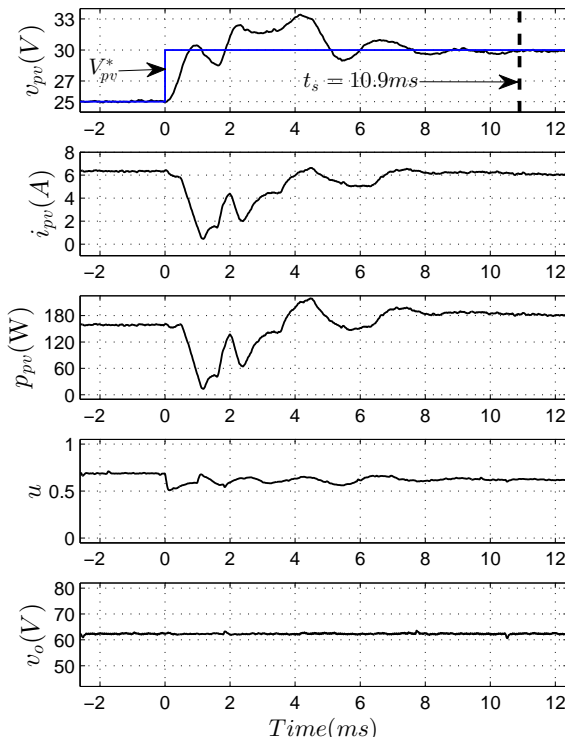

(b) 5 V Variation - Controller c_1

(b) 5 V Variation - Controller c_2

**FIGURE 7.** Set-Point Variation Tests - Controller c_1

FIGURE 8. Set-Point Variation Tests - Controller $c_1 2$.

figures, we can observe a stable regulation with expected transient scenarios enhanced. Hence, despite any disturbance, the PV voltage tends to the voltage reference $v_{pv}^* = 30\,\mathrm{V}$.
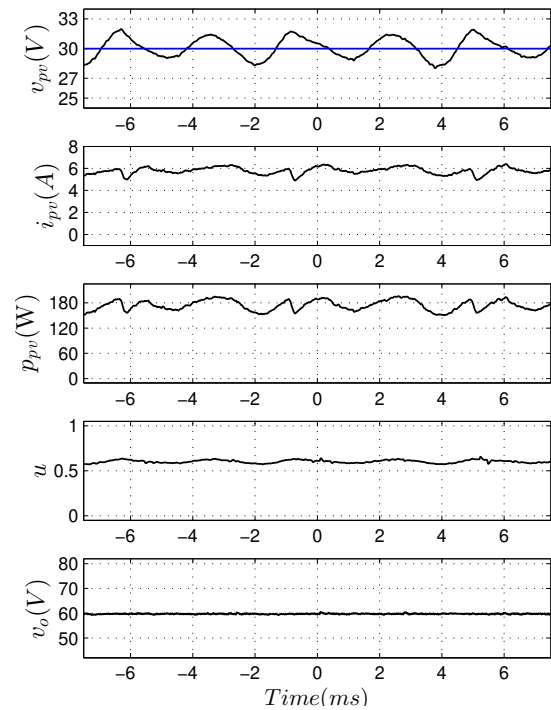
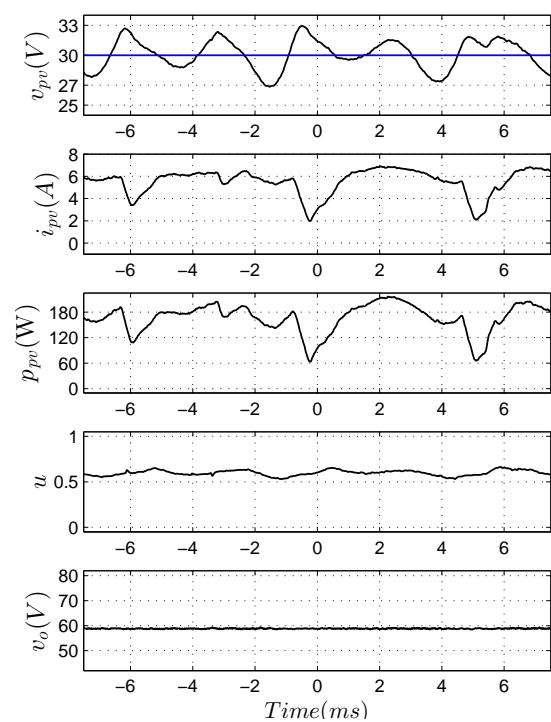Finally, to complete the tests we consider the two unstable controllers for a constant regulation with $v_{pv}^* = 30\,\mathrm{V}$ and

IEEE *Access*
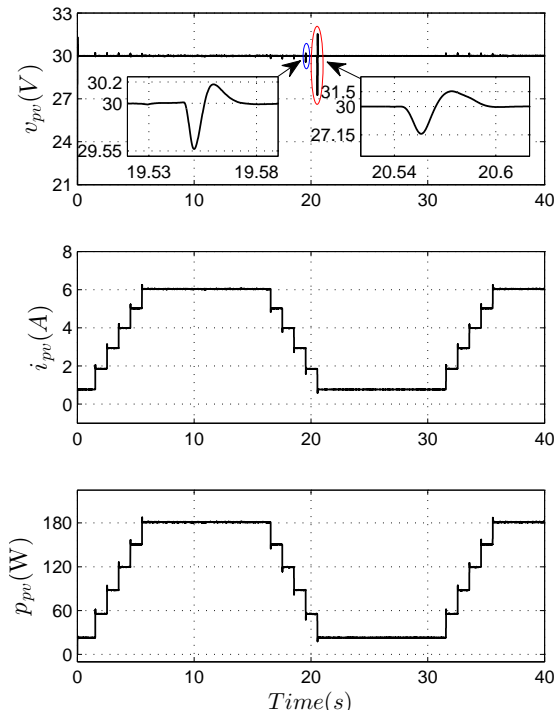
(a) Controller c_1 Under Irradiance Disturbances
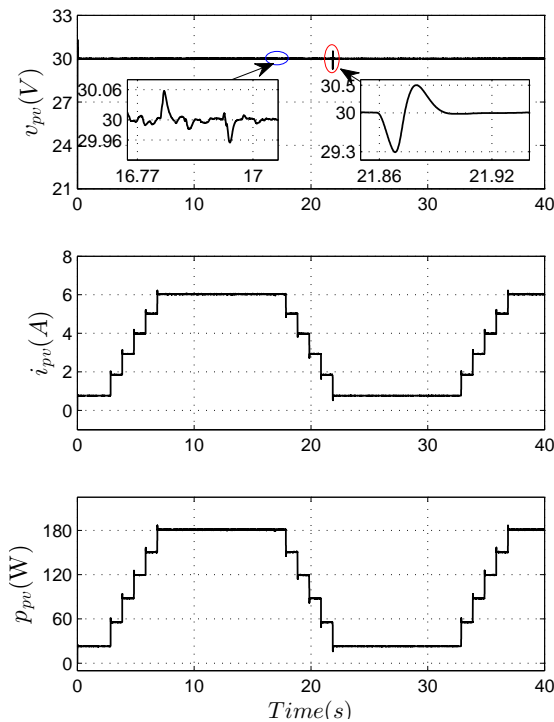
(b) Controller c_2 Under Irradiance Disturbances

FIGURE 9. Controller Performance Tests.

(a) Unstable Controller c_3

(b) Unstable Controller c_4

FIGURE 10. Controller Performance Tests.

without any transient condition. In this vein, as expected, Fig. 10 illustrates the unstable responses. One may notice from Table 4 that the experiment shown in Fig. 10a has a lack of the delayed action, illustrating that the proposed controller needs the "gain-delay block" in order to have an asymptotically stable behavior. In a similar fashion, it is

interesting to observe how the design analysis suggests the use of a negative gain k_δ (for c_1), in which if we switch the sign to this gain, results in an unstable behavior, as can be appreciated from Fig. 10b.

C. GRAPHICAL COMPARISONS

In general, in model-based control schemes implementations there are several factors that may impact their performance, between the most important it can be mentioned: physical control computation, controller parameters tuning, non-modeled dynamics, and model parameters uncertainty. Also, measuring and comparing different control schemes is not always an obvious task if more than one performance feature is considered. With these facts in mind, in this section, a graphics-based qualitative comparative consisting of a radar chart is proposed and explained in detail in the following lines.

First of all, this radar chart is shown in Fig. 11 and consists of a three-level performance metrics (poor, decent, good) and uses three performance features: settling time, number of required measurements, and simplicity of the controller structure. The first two features are directly borrowed from Table 1, whereas the third one is the authors' opinion regarding the computational complexity. Considering a particular control strategy, the main idea is to draw a triangle in which corners represent the performance of such in each feature. Being a poor performance the most inner corners and a good one being the most outer ones.

As discussed in the Introduction, and explicitly shown in Table 1, there are a variety of strategies applied to PV systems along with a similar approach to the one studied in this paper. In the proposed comparison, we consider only three of them along with the one proposed in this work. To summarize, Fig. 11 depicts four polygons with different contours corresponding to each control law: sliding mode control [6] (dashed contour), PI$\delta-$controller (solid contour/shaded one), adaptive control [30] (double dotted contour), back-stepping/sliding mode strategy [7] (dotted contour).

To conclude, from Fig. 11 we highlight the following observations:

1) The backstepping/sliding mode strategy used in [7] has a conservative performance in all considered features. In other words, is the slowest one and requires the most out of measurement hardware and computational complexity.

2) The sliding mode strategy presented in [6] is the fastest one by using some decent hardware and software requirements.

3) The proposed delay-based controller is the simplest of all of them in its computation and implementation. However, it has a decent settle time but is not the fastest one.

In addition, it is worth mentioning that [6] requires an extra current sensor i_{pv} in comparison with the PIδ-based controller.

VI. CONCLUDING REMARKS

A non–linear delay–based control scheme is proposed to solve the closed-loop stabilization problem of a MPPT-Boost
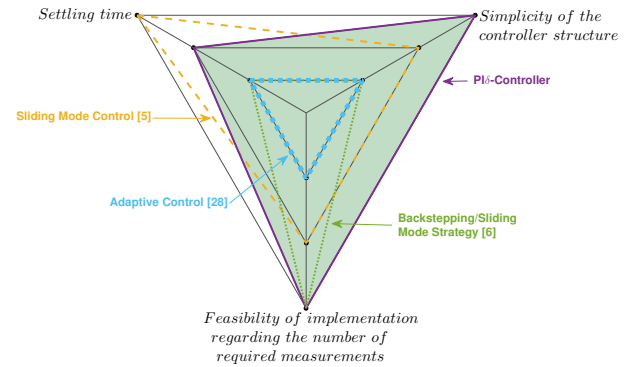
FIGURE 11. Radar Diagram Illustrating the Performance of the Controllers on Various Assessment Aspects Related to the Photovoltaic Dynamics.

Converter as a PV system. The conception of such an idea is formed by two control strategies. First, an output feedback linearization technique transforming the overall system into a two-degree oscillators chain. Second, a proportional-delayed controller with an integral action is proposed to stabilize such a chain. This idea is the conceptual contribution of the paper and which application is the main technical one. Formed likewise, by two steps presented in this work. On one hand, the zero dynamics internal stability analysis developed through well-known Lyapunov stability criteria. On the other hand, the design of the delay-based linear controller, this consisting of a detailed analysis of the characteristic roots (of closed-loop previously linearized system) behavior as the controller's parameters are varied. Also, the fragility problem for the PIδ is discussed, and an auxiliary result to measure the robustness of the controller against parametrical uncertainties and variations is presented. In addition, experimental results concerning set-point changes (mimicking a P&O tracking system) and evaluation under transient conditions are addressed using only one voltage sensor in an isolated PV system application. Finally, from an overall review of this work, it is worth enhancing two main advantages. First, the lack of need for a current sensor in the loop in comparison with the literature presented in Tab. 1. Second, the avoidance of a derivative action in the PID–alike linear controller, which is replaced by a delayed action.

REFERENCES

[1] A. Kihal, F. Krim, A. Laib, B. Talbi, H. Afghoul An Improved MPPT Scheme Employing Adaptive Integral Derivative Sliding Mode Control for Photovoltaic Systems Under Fast Irradiation Changes. ISA Transactions, 87(1):297-306, 2019.

[2] W. Altmann and D. Macdonald. Practical Process Control for Engineers and Technicians. Elsevier/Newnes, 2005.

[3] K. J. Aström and T. Hägglund. PID Controllers: Theory, Design, and Tuning. Instrument Society of America, Research Triangle Park, NC, 2 edition, 1995.

[4] J. Bai, Y. Cao, Y. Hao, Z. Zhang, S. Liu, F. Cao. Characteristic output of PV systems under partial shading or mismatch conditions. Solar Energy, 112:41–54, 2015.

[5] E. I. Batzelis, G. E. Kampitsis, S. A. Papathanassiou, and S. N. Manias. Direct mpp calculation in terms of the single-diode pv model parameters. IEEE Transactions on Power Electronics, 30(1):2226-2336, 2015.

[6] E. Bianconi, J. Calvente, R. Giral, E. Mamarelis, G. Petrone, C. A. Ramos-Paja, G. Spagnuolo, and M. Vitelli. A fast current-based mppt technique employing sliding mode control. IEEE Transactions on Industrial Electronics, 60(3):1168-1178, 2013.

[7] K. Dahech, M. Allouche, T. Damak, and F. Tadeo. Backstepping sliding mode control for maximum power point tracking of a photovoltaic system. Electric Power Systems Research, 143:182-188, 2017.

[8] E. Dallago, A. Liberale, D. Miotti, and G. Venchi. Direct mppt algorithm for pv sources with only voltage measurements. IEEE Transactions on Power Electronics, 30(12):6742-6750, 2015.

[9] D. R. Espinoza-Trejo, E. Bárcenas-Bárcenas, D. U. Campos-Delgado, and C.H. De Angelo. Voltage-oriented input-output linearization controller as maximum power point tracking technique for photovoltaic systems. IEEE Transactions on Industrial Electronics, 2014.

[10] D. González-Montoya, C. A. Ramos-Paja, and R. Giral. Improved design of sliding mode controllers based on the requirements of mppt techniques. IEEE Transactions on Power Electronics, 31(1):235-247, 2016.

[11] H. Guggenheimer. Differential Geometry. Dover, New York, NY, 1977.

[12] J. E. Hernández-Díez, E. J. González-Galván, C. F. Méndez-Barrios, S. I. Niculescu, A. Loredo-Flores, and R. I. Hernández-Molinar. A bilateral control scheme of a haptic-virtual system using proportional-delayed controllers. AMRob Journal, Robotics: Theory and Applications, 49(2):1-7, 2016.

[13] J. E. Hernández-Díez, E. J. González-Galván, C. F. Méndez-Barrios and S. I. Niculescu, Practical Guidelines for Tuning PD and PI Delay-Based Controllers. 15th IFAC Workshop on Time Delay Systems. Sinaia, Romania, 2019.

[14] R. Khanna, Q. Zhang, W. E. Stanchina, G. F. Reed, and Z.-H. Mao. Maximum power point tracking using model reference adaptive control. IEEE Transactions on Power Electronics, 29(3):1490-1499, 2014.

[15] M. Killi and S. Samanta. Modified perturb and observe mppt algorithm for drift avoidance in photovoltaic systems. IEEE Transactions on Industrial Electronics, 62(9):5549-5559, 2015.

[16] S. Lyden and M. E. Haque. Maximum power tracking techniques for photovoltaic systems: A comprehensive review and comparative analysis. Renewable & Sustainable Energy Reviews, 52:1504–1518, 2015.

[17] M. Metry, M. B. Shadmand, R. S. Balog, and H. Abu-Rub. Mppt of photovoltaic systems using sensorless current-based model predictive control. IEEE Transactions on Industry Applications, 2017.

[18] W. Michiels and S.-I. Niculescu. Stability, Control, and Computation for Time-Delay Systems. An Eigenvalue-Based Approach. Advances in Design and Control. SIAM, Philadelphia, 2014.

[19] J. Neimark. D-subdivisions and spaces of quasi-polynomials. Prikl. Math. Mech., 10:349-380, 1949.

[20] S.-I. Niculescu and W. Michiels. Stabilizing a chain of integrators using multiple delays. IEEE Trans. Aut. Control, 49(5):802-807, 2004.

[21] R. Pradhan and B. Subudhi. Double integral sliding mode mppt control of a photovoltaic system. IEEE Transactions on Control Systems Technology, 24(1):285-292, 2016.

[22] A. Ramírez, S. Mondié, R. Garrido, and R. Sipahi. Design of proportional-integral-retarded (pir) controllers for second-order lti systems. IEEE Transactions On Automatic Control, 61(6):1688-1693, 2016.

[23] M. H. Rashid. Power Electronics: Devides, Circuits and Applications. Pearson, 2013.

[24] M. Rassol and Ali-Badamchizadeh. Adaptative passivity-based control of a photovoltaic system. IEEE Journal of Photovoltaics, 6(2):532-539l, 2016.

[25] E. Romero-Cadaval, B. Francois, M. Malinowsky, and Q. C. Zhong. Grid-connected photovoltaic plants: An alternative energy source, replacing conventional sources. IEEE Industrial Electronics Magazine, 9(1):18-32, 2009.

[26] S. S. Sastry. Nonlinear Systems: Analysis, Stability and Control. Springer, 1999.

[27] J. M. Shen, H. L. Jou, and J. C. Wu. Transformers-less three-port grid-connected power converter for distribution power generation system with dual renewavle energy sources. IET Power Electronics, 5(3):501-509, 2011.

[28] H. Suh and Z. Bien. Use of time-delay actions in the controller design. IEEE Transactions On Automatic Control, 25(3):600-603, 1980.

[29] J.C. Teo, R.H.G. Tan, V.H. Mok, V.K. Ramachandaramurthy and C. Tan. Impact of Partial Shading on the P-V Characteristics and the Maximum Power of a Photovoltaic String. Energies, 11(7):1860, 2018.

[30] A. Urtasun, P. Sanchis, and L. Marroyo. Adaptive voltage control of the dc/dc boost stage in pv converter with small input capacitor. IEEE Transactions on Power Electronics, 28(11):5038-5048, 2015.

[31] P. Vázquez, A. Alviso, V.-M. Tovar, and D.-R. Espinoza-Trejo. High-performance controller for a boost dc/dc converter in photovoltaic mppt systems by using a pic32mz microcontroller. Currently Submitted to Energies, 2018.

JOSÉ-ENRIQUE HERNÁNDEZ-DÍEZ was born in San Luis Potosí Mexico. He received the B.S. degree in Mechatronics engineering and the M. Eng. in electrical engineering from the Universidad Autónoma de San Luis Potosí, San Luis Potosí (UASLP), in 2008 and 2016, respectively. Currently he is enrolled in a joint PhD program between l'Université Paris-Saclay and the UASLP. His main research interests are directly related to the design of low-complexity controllers for industrial applications and, in particular, the stability of delayed dynamics and applications to power electronics and robotics.

FERNANDO MÉNDEZ-BARRIOS received the M.Sc. degree in Control Theory from the Center for Research and Advanced Studies of the National Polytechnic Institute (CINVESTAV), in 2005, and the Ph.D. degree from the University of Paris-Sud XI in 2011. Since 2012, he is Professor in the Mechatronics Department, at the Autonomous University of San Luis Potosí (UASLP). Currently, he is serving as Associate Chair of the Graduate Program in Electrical Engineering. He has authored and co-authored over 30 peer-reviewed publications. His research interest belongs to the qualitative theory of dynamical systems and its application in control problems. More precisely, he is interested by the qualitative analysis of the effects induced by the parameters on the systems dynamics with a particular emphasis on delays as well as the applications of these techniques to the control of robotic and teleoperation systems.

SILVIU-IULIAN NICULESCU received the B.S. degree from the Politehnica University of Bucharest, Romania, in 1992, the M.Sc. and Ph.D. degrees from the Institut National Polytechnique de Grenoble, France, in 1993 and 1996, respectively, and the French Habilitation degree from the Université de Technologie de Compiègne, in 2003, all in automatic control. He is currently Research Director with the French National Center for Scientific Research (CNRS) working at the Laboratoire des Signaux et Systèmes, a joint Research Unit of CNRS with Université Paris-Saclay and CentraleSupélec, located at Gif-sur-Yvette. Currently, he is the Chair of the IFAC Technical Committee 2.2. on "Linear Control Systems" (since 2017). He is the founding and the Editor-in-Chief of the series "Advances in delay and dynamics" (ADD@S) at Springer Nature (since 2012). He also served as an Associate Editor for several journals in Control area, including the IEEE TRANSACTIONS ON AUTOMATIC CONTROL from 2003 to 2005. He was also the Head of L2S from 2010 to 2019. He has authored or co-authored 10 books and over 550 scientific papers. He has been the responsible of the IFAC Research Group on "Time Delay Systems" from 2007 to 2017. He is the recipient of the CNRS Silver and Bronze Medals for scientific research and the Ph.D. Thesis Award from INPG, Grenoble, France, in 2011, 2001, and 1996, respectively. His research interests include delay systems, robust control, operator theory, and numerical methods in optimization, and their applications to the design of engineering systems.

ERNESTO BÁRCENAS-BÁRCENAS was born in San Luis Potosí, Mexico. He received the B.S. degree in electronics engineering from the Universidad Autónoma de San Luis Potosí, San Luis Potosí, in 2000 and the M.Sc. and Ph.D. degrees in power electronics from the Centro Nacional de Investigación y Desarrollo Tecnológico, Cuernavaca, Mexico, in 2002 and 2008, respectively. Since 2010, he has been with the Coordinación Académica Región Altiplano of the Universidad Autónoma de San Luis Potosías a full time professor in the Mechatronics Department. He has authored or co-authored over 10 peer-reviewed publications. His main research interests include power electronics for renewable energy applications, ac–dc conversion, and electric machine drives.

• • •